Progress In Electromagnetics Research B, Vol. 68, 17–33, 2016

Design of Dual-Band Filters with Individually Controllable Passband Responses and Orders

Xiaofeng Sun* **and Eng Leong Tan**

Abstract—This paper presents a novel design of dual-band filters with individually controllable passband responses and orders. Besides the center frequency and bandwidth, the response and order of each passband can be different and controlled individually. The dual-band filter is formed by synthesizing each filter element (resonator, inverter) one by one, exploiting the corresponding individual single-band filters design tables/formulas for different prototype responses and orders. Trisection stepped-impedance resonators (TSSIR) are adopted with novel considerations as dual-band resonators, whose additional design parameters could help to realize the required in-band responses (resonances, slope parameters) and improve simultaneously the out-of-band performances (transmission zeros of TSSIR). Furthermore, they can be used to design a dual-band filter with far separation between two passbands. Meanwhile, stepped-impedance inverters are chosen as dual-band inverters with novel additional conditions to obtain symmetric passbands, which can also provide different inverter immittance parameters J/K at two center frequencies when the response or order of each passband is different. To illustrate the two passbands being controlled individually, two dual-band filters with different orders and responses are demonstrated.

1. INTRODUCTION

With the rapid developments of modern wireless and mobile communications, a bandpass filter becomes a more important component in RF and microwave communication systems and applications [1–4]. The requirements of microwave filters also become more stringent. Compared with multiple single-band bandpass filters, multi-band bandpass filters with dual-band or tri-band attract more researchers' attention.

Most previous works claimed that the proposed dual-band filters were controllable [5–19]. However, their "controllability" was merely in center frequencies and bandwidths, not in detailed responses or orders of individual bands. Actually, for dual-band filter design, we should not be complacent with only center frequencies and bandwidths, but should also consider, specify and control the responses in more detail including prototypes and orders. In [5, 6], some numerical approaches were proposed for dual-band filter design, which relied heavily on some general optimization of the whole filter. There was no guarantee that the orders or prototypes would be realized eventually (especially for poor initial values, or ill offsprings not constrained well enough, etc.) In [7, 8], dual-band responses were realized by splitting a wide passband with a narrow stopband, using the bandpass and bandstop filters in cascade, or the bandpass and bandstop resonators in parallel connections. Since the dual-band responses were split from a common wide passband, each of the dual bands cannot be controlled flexibly in the individual orders and prototype responses. In [9], a dual-band frequency transformation was proposed. However, the limitation of the proposed design was that the center frequency of the stopband cannot deviate

Received 23 March 2016, Accepted 2 May 2016, Scheduled 11 May 2016
* Corresponding author: Xiaofeng Sun (sunxf@ntu.edu.sg).
The authors are with the School of Electrical and Electronic Engineering, Nanyang Technological University, 50 Nanyang Avenue, 639798, Singapore.

far from that of the passband. Moreover, the prototypes and orders of both passbands were the same. In [10], based on dual-behavior resonator (DBR) realized by parallel open stubs, a dual-band response was created. The DBR mainly concerns about transmission zeros in stopbands and not so much about the total transmission of interest in passbands. In [11] and [12], a dual frequency transformation was proposed whereby a lowpass filter is first transformed to a single-band bandpass filter and then further transformed to a dual-band bandpass filter. Thus, the responses and orders of the proposed dual-band filter cannot be controlled individually. In [13], a dual-band bandpass filter with p-i-n diodes was proposed. In [14], a multilayer dual-band balun filter was proposed. In [15], a dual-band filter based on asymmetric quarter-wavelength resonator pairs with shared via-hole ground was proposed. [13–15] claimed that the dual-band filters were controllable. Again, the "controllability" was in center frequencies and bandwidths, but not in responses or orders of individual bands.

Considering the filter elements, in most previous resonators, only resonant conditions and slope parameters were considered [11, 16–19]. That means only in-band responses were controlled, and no detailed responses or orders of individual bands could be specified or designed. In [11, 16, 17], dual-band filters with a controllable second passband were designed using quarter wavelength shorted stubs as resonators, whose harmonics cannot be controlled. Thus, it is difficult to control the out-of-band performance of the quarter wavelength shorted stubs. Meanwhile, the stepped-impedance resonators (SIRs) were used to design dual-band filters in [18, 19]. They allow easy control of resonant frequencies by adjusting their characteristic impedance ratios and the electrical length ratios [20], However, only in-band responses (resonances, slope parameters) of SIRs were considered, while the out-of-band performances (transmission zeros) of SIRs were not considered.

Some inverters were also proposed in previous works [10, 11, 16–19]. In [10], the inverter used was quarter-wavelength transmission line, but such quarter-wavelength was not specified at which (single) frequency and its fixed characteristic impedance limited the flexibility in the order/response of dual-band filter. In [11], many inverters were introduced and realized by quarter-wavelength transmission lines, but these are not general dual-band inverters. In [16, 17], the electrical lengths of the stubs of inverters were limited to be same as those of resonators. In [18, 19], the omission of inverter stubs could save space but at a cost of reducing the bandwidth. Moreover, the dual-band inverter used in [16–19] can only provide the same inverter immittance parameters J/K, which also limited the flexibility in order/response of dual-band filter if the required J/K values at both bands need to be different.

It should be noted that the periodicity in the response of quarter-wavelength transmission line and stub also limits the separation between two passbands [10, 11, 16–19]. Fewer design parameters of bisection SIR also limited the flexibility of the dual-band filter design, especially for farther separation between two bands due to fabrication limitations [9]. In [21], a dual-band filter with widely separated passbands was proposed and implemented by non-planar cylindrical cavities. Still, its separation may not be wide enough. Although [22] and [23] proposed the trisection stepped-impedance resonator (TSSIR) and the stepped-impedance inverter (SII), the separations between two passbands were not very great. Each passband response was not in different prototype nor different order. In [24], each passband response was in different prototype, but the orders of individual passbands were the same.

This paper presents a novel design of dual-band filters with individually controllable passband responses and orders. Besides the center frequency and bandwidth, the response and order of each passband can be different and controlled individually. The dual-band filter is formed by synthesizing each filter element (resonator, inverter) one by one, exploiting the corresponding individual single-band filters design tables/formulas for different prototype responses and orders. Trisection stepped-impedance resonators are adopted with novel considerations as dual-band resonators, whose additional design parameters could help to realize the required in-band responses (resonances, slope parameters) and improve simultaneously the out-of-band performances (transmission zeros of TSSIR). Furthermore, they can be used to design a dual-band filter with far separation between two passbands. Meanwhile, stepped-impedance inverters are chosen as dual-band inverters with novel additional conditions to obtain symmetric passbands, which can also provide different inverter immittance parameters J/K at two center frequencies when the response or order of each passband is different. To illustrate the two passbands being controlled individually, two dual-band filters with different orders and responses are demonstrated.

2. DUAL-BAND FILTER DESIGN

In this section, the dual-band filter is formed by synthesizing each filter element (resonator, inverter) one by one, exploiting the corresponding individual single-band filters design tables/formulas for different prototype responses and orders.

2.1. Single-Band Resonators and Inverters

We shall first summarize one such single-band filter element design applicable for individual bands of dual-band filter.

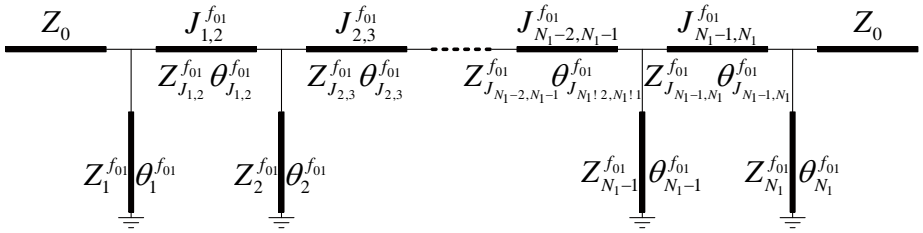

Figure 1. Geometry of a N_1-th single-band bandpass filter.

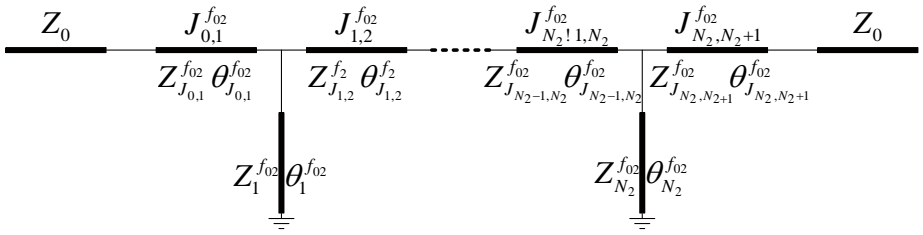

Figure 2. Geometry of a N_2-th single-band bandpass filter.

A single-band bandpass filter can be realized by quarter-wavelength microstrip stubs and lines, which are serving as resonators and inverters as shown in Fig. 1 and Fig. 2 [1–4]. In Fig. 1, the proposed filter can be recognized as N_1-th order structure with passband center frequency f_{01}. One can calculate the parameters of the structure including the characteristic impedances of stub resonators ($Z_{n_1}^{f_{01}}$, where $n_1 = 1$ to N_1.) by

$$\begin{aligned}
\theta^{f_{01}} &= \frac{\pi}{2}\left(1 - \frac{\Delta^{f_{01}}}{2}\right), \\
M_{n_1,n_1+1}^{f_{01}} &= \sqrt{\left(J_{n_1,n_1+1}^{f_{01}} Z_0\right)^2 + \left(\frac{h^{f_{01}} g_0^{f_{01}} g_1^{f_{01}} \tan\theta^{f_{01}}}{2}\right)^2} \quad \text{for } n_1 = 1 \text{ to } N_1 - 1, \\
\frac{1}{Z_1^{f_{01}}} &= \frac{g_0^{f_{01}}}{Z_0}\left(1 - \frac{h^{f_{01}}}{2}\right) g_1^{f_{01}} \tan\theta^{f_{01}} + \left(\frac{M_{1,2}^{f_{01}}}{Z_0} - J_{1,2}^{f_{01}}\right), \\
\frac{1}{Z_{N_1}^{f_{01}}} &= \frac{1}{Z_0}\left(g_{N_1}^{f_{01}} g_{N_1+1}^{f_{01}} - g_0^{f_{01}} g_1^{f_{01}} \frac{h}{2}\right) \tan\theta^{f_{01}} + \left(\frac{M_{N_1-1,N_1}^{f_{01}}}{Z_0} - J_{N_1-1,N_1}^{f_{01}}\right), \\
\frac{1}{Z_{n_1}^{f_{01}}} &= \frac{1}{Z_0}\left(M_{n_1-1,n_1}^{f_{01}} + M_{n_1+1,n_1}^{f_{01}}\right) - J_{n_1-1,n_1}^{f_{01}} - J_{n_1,n_1+1}^{f_{01}} \quad \text{for } n_1 = 2 \text{ to } N_1 - 1.
\end{aligned} \tag{1}$$

and the characteristic impedances of inverters ($Z^{f_{01}}_{J_{k_1,k_1+1}}$, where $k_1 = 1$ to $N_1 - 1$.) by

$$\begin{aligned} Z^{f_{01}}_{J_{1,2}} &= \frac{1}{J^{f_{01}}_{1,2}} = \frac{Z_0}{g_0^{f_{01}}}\sqrt{\frac{g_2^{f_{01}}}{h^{f_{01}} g_1^{f_{01}}}}, \\ Z^{f_{01}}_{J_{N_1-1,N_1}} &= \frac{1}{J^{f_{01}}_{N_1-1,N_1}} = \frac{Z_0}{g_0^{f_{01}}}\sqrt{\frac{g_0^{f_{01}} g_{N_1-1}^{f_{01}}}{h^{f_{01}} g_1^{f_{01}} g_{N_1+1}^{f_{01}}}}, \\ Z^{f_{01}}_{J_{k_1,k_1+1}} &= \frac{1}{J^{f_{01}}_{k_1,k_1+1}} = Z_0\frac{\sqrt{g_{k_1}^{f_{01}} g_{k_1+1}^{f_{01}}}}{h^{f_{01}} g_0^{f_{01}} g_1^{f_{01}}} \quad \text{for } k_1 = 2 \text{ to } N_1 - 2. \end{aligned} \tag{2}$$

Note that Z, J, Δ, θ, g and h with superscript f_{01} merely signify that they are the parameters of a single-band filter whose center frequency is f_{01}, it does not mean that they are dependent on f_{01}. $\Delta^{f_{01}}$ is defined as the fractional bandwidth. $g^{f_{01}}$ is the element value, which can be Chebyshev or Butterworth lowpass prototype, etc. $h^{f_{01}}$ is a constant which can adjust the admittance level in the interior of the filter. The electrical lengths of the stub resonators ($\theta^{f_{01}}_{n_1}$, where $n_1 = 1$ to N_1) and inverters ($\theta^{f_{01}}_{J_{k_1,k_1+1}}$, where $k_1 = 1$ to $N_1 - 1$) are 90° at f_{01}. Thus, the susceptance slope parameters of these stubs at f_{01} can be expressed by

$$b^{f_{01}}_{n_1} = \frac{f_{01}}{2}\frac{dY^{f_{01}}_{in_{n_1}}(f)}{df}\bigg|_{f=f_{01}} = \frac{\pi}{4Z^{f_{01}}_{n_1}}. \tag{3}$$

where $Y^{f_{01}}_{in_{n_1}}$ are the input admittances of the quarter wavelength stubs with characteristic impedances $Z^{f_{01}}_{n_1}$.

Similarly, Fig. 2 shows a N_2-th order structure with external feeding lines of characteristic impedances $Z^{f_{02}}_{J_{0,1}}, Z^{f_{02}}_{J_{N_2,N_2+1}} = Z_0$ and electrical lengths $\theta^{f_{02}}_{J_{0,1}}, \theta^{f_{02}}_{J_{N_2,N_2+1}} = 90°$ at passband center frequency f_{02}. Here N_2 can be different from N_1, e.g., $N_2 < N_1$. The characteristic impedances of the stub resonators ($Z^{f_{02}}_{n_2}$, where $n_2 = 1$ to N_2) and inverters ($Z^{f_{02}}_{J_{k_2,k_2+1}}$, where $k_2 = 1$ to $N_2 - 1$) can also be calculated by replacing f_{01} with f_{02} in Eqs. (1) and (2). Likewise using Eq. (3), the susceptance slope parameters of stubs ($b^{f_{02}}_{n_2}$) at f_{02} can also be obtained.

2.2. Dual-band Resonators and Inverters

To implement a dual-band filter with two individually controllable passbands, we shall use trisection stepped-impedance resonators (TSSIR) as dual-band resonators due to its controllable resonances, and stepped-impedance inverters (SII) as dual-band inverters, as shown in Fig. 3. The TSSIR should not only have two resonances (f_{R1}, f_{R2}) at two required frequencies of the individual single-bands, but should also satisfy the corresponding susceptance slope parameters as below:

• $N_1 \geq N_2$:

– For central $n = \text{floor}(\frac{N_1-N_2}{2}) + 1$ to $\text{floor}(\frac{N_1+N_2}{2})$:

$$Y_{in_n}(f_{R1})|_{f_{R1}=f_{01}} = 0, \tag{4}$$

$$Y_{in_n}(f_{R2})|_{f_{R2}=f_{02}} = 0, \tag{5}$$

$$b_n(f_{R1})|_{f_{R1}=f_{01}} = b^{f_{01}}_{n_1}, \quad n_1 = n \tag{6}$$

$$b_n(f_{R2})|_{f_{R2}=f_{02}} = b^{f_{02}}_{n_2}, \quad n_2 = n - (N_1 - N_2)/2 \tag{7}$$

– For peripheral n =1 to floor($\frac{N_1-N_2}{2}$), and floor($\frac{N_1+N_2}{2}$)+1 to N_1:

$$Y_{in_n}(f_{R1})|_{f_{R1}=f_{01}} = 0, \tag{8}$$
$$Y_{in_n}(f_{R2})|_{f_{R2}=f_s} = 0, \quad f_s \gg f_{02} \tag{9}$$
$$b_n(f_{R1})|_{f_{R1}=f_{01}} = b_n^{f_{01}}, \tag{10}$$
$$b_n(f_{R2})|_{f_{R2}=f_s} = b^{f_s}. \tag{11}$$

• $N_1 \leq N_2$:
– For central n = floor($\frac{N_2-N_1}{2}$) + 1 to floor($\frac{N_1+N_2}{2}$):

$$Y_{in_n}(f_{R1})|_{f_{R1}=f_{01}} = 0, \tag{12}$$
$$Y_{in_n}(f_{R2})|_{f_{R2}=f_{02}} = 0, \tag{13}$$
$$b_n(f_{R1})|_{f_{R1}=f_{01}} = b_{n_1}^{f_{01}}, \quad n_1 = n - (N_2 - N_1)/2 \tag{14}$$
$$b_n(f_{R2})|_{f_{R2}=f_{02}} = b_{n_2}^{f_{02}}, \quad n_2 = n \tag{15}$$

– For peripheral n =1 to floor($\frac{N_2-N_1}{2}$), and floor($\frac{N_1+N_2}{2}$)+1 to N_2:

$$Y_{in_n}(f_{R1})|_{f_{R1}=f_s} = 0, \quad f_s \ll f_{01} \tag{16}$$
$$Y_{in_n}(f_{R2})|_{f_{R2}=f_{02}} = 0, \tag{17}$$
$$b_n(f_{R1})|_{f_{R1}=f_s} = b^{f_s}, \tag{18}$$
$$b_n(f_{R2})|_{f_{R2}=f_{02}} = b_n^{f_{02}}. \tag{19}$$

If $N_1 \neq N_2$, the central TSSIRs are used to realize both passbands, and the peripheral TSSIRs are employed to realize the passband with higher order. The peripheral TSSIRs should also control their resonances to avoid interfering the passband with lower order.

As the dual-band inverters, the SII should have two inverter admittance parameters J at two center frequencies as below:
• $N_1 \geq N_2$:
– For central k = floor($\frac{N_1-N_2}{2}$)+1 to floor($\frac{N_1+N_2}{2}$)-1:

$$J_{k,k+1}(f)|_{f=f_{01}} = J_{k_1,k_1+1}^{f_{01}}, \quad k_1 = k, \tag{20}$$
$$J_{k,k+1}(f)|_{f=f_{02}} = J_{k_2,k_2+1}^{f_{02}}, \quad k_2 = k - \text{floor}\left(\frac{N_1 - N_2}{2}\right) \tag{21}$$

– For peripheral k = 1 to floor($\frac{N_1-N_2}{2}$), and floor($\frac{N_1+N_2}{2}$) to N_1-1:

$$J_{k,k+1}(f)|_{f=f_{01}} = J_{k,k+1}^{f_{01}}, \tag{22}$$
$$J_{k,k+1}(f)|_{f=f_{02}} = 1/Z_0. \tag{23}$$

• $N_1 \leq N_2$:
– For central k = floor($\frac{N_2-N_1}{2}$)+1 to floor($\frac{N_1+N_2}{2}$)-1:

$$J_{k,k+1}(f)|_{f=f_{01}} = J_{k_1,k_1+1}^{f_{01}}, \quad k_1 = k - \text{floor}\left(\frac{N_2 - N_1}{2}\right) \tag{24}$$
$$J_{k,k+1}(f)|_{f=f_{02}} = J_{k_2,k_2+1}^{f_{02}}, \quad k_2 = k \tag{25}$$

– For peripheral k = 1 to floor($\frac{N_2-N_1}{2}$), and floor($\frac{N_1+N_2}{2}$) to N_2-1:

$$J_{k,k+1}(f)|_{f=f_{01}} = 1/Z_0, \tag{26}$$
$$J_{k,k+1}(f)|_{f=f_{02}} = J_{k,k+1}^{f_{02}}. \tag{27}$$

If the prototypes are different ($g_{k_1}^{f_{01}} \neq g_{k_2}^{f_{02}}$), SII can provide different inverter immittance parameters J/K at two center frequencies if the response or order of each band is different.

To be more specific for subsequent discussion, the separation between two passbands is defined in terms of the center frequencies of the first (f_{01}) and second (f_{02}) passbands as

$$\delta_{12} = \frac{f_{02} - f_{01}}{\sqrt{f_{01} f_{02}}}. \tag{28}$$

Such definition may be extended for tri-band bandpass filter and beyond, e.g., the separation between the second and third passbands can be written as

$$\delta_{23} = \frac{f_{03} - f_{02}}{\sqrt{f_{02} f_{03}}}. \tag{29}$$

where f_{03} is the center frequency of the third passband not within scope.

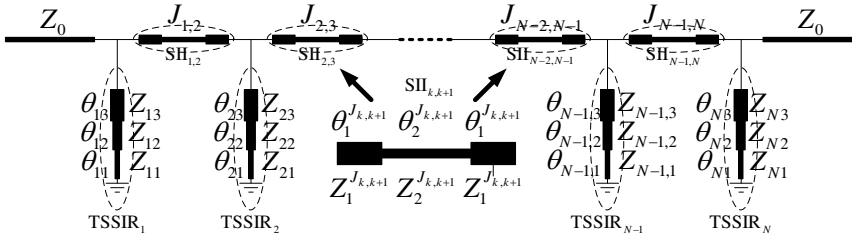

Figure 3. Dual-band filter using TSSIRs and SIIs.

2.3. Trisection Stepped-Impedance Resonator

A trisection stepped-impedance resonator (TSSIR) is used instead of a quarter-wavelength or bisection stepped-impedance stub resonator to implement dual-band resonator. The resonant condition of a short-ended TSSIR can be expressed as

$$\begin{aligned}
Y_{in_p}(f) =& j\frac{N_{Yin_p}(f)}{Z_{p3} D_{Yin_p}(f)} = 0, \\
N_{Yin_p}(f) =& \left(Z_{p1} Z_{p3} \tan\left(\theta_{p1}\frac{f}{f_{01}}\right) \tan\left(\theta_{p2}\frac{f}{f_{01}}\right) + Z_{p1} Z_{p2} \tan\left(\theta_{p1}\frac{f}{f_{01}}\right) \tan\left(\theta_{p3}\frac{f}{f_{01}}\right) \right. \\
& \left. + Z_{p2}^2 \tan\left(\theta_{p2}\frac{f}{f_{01}}\right) \tan\left(\theta_{p3}\frac{f}{f_{01}}\right) - Z_{p2} Z_{p3} \right), \\
D_{Yin_p}(f) =& \left(Z_{p1} Z_{p2} \tan\left(\theta_{p1}\frac{f}{f_{01}}\right) + Z_{p2}^2 \tan\left(\theta_{p2}\frac{f}{f_{01}}\right) + Z_{p2} Z_{p3} \tan\left(\theta_{p3}\frac{f}{f_{01}}\right) \right. \\
& \left. - Z_{p1} Z_{p3} \tan\left(\theta_{p1}\frac{f}{f_{01}}\right) \tan\left(\theta_{p2}\frac{f}{f_{01}}\right) \tan\left(\theta_{p3}\frac{f}{f_{01}}\right) \right),
\end{aligned} \tag{30}$$

where Z_{pq} is the characteristic impedance of the q-th section of TSSIR$_p$, and θ_{pq} is corresponding to electrical length at the first resonant frequency f_{01}. Referring to Fig. 3, subscript p denotes the shunt branch of filter, which is from 1 to $\max(N_1, N_2)$. Subscript q indicates the section of TSSIR, which is from 1 to 3, starting from the short-circuit end.

The definition of the susceptance slope parameter can provide a convenient means for relating the resonance property of a resonator circuit to that of a simple lumped equivalent circuit [2, 3]. Thus, when we replace quarter-wavelength resonator by TSSIR, the susceptance slope parameter of TSSIR should be made equal to that of the single-band quarter-wavelength resonator. The susceptance slope parameters of the proposed TSSIR is [22]

$$b_p(f) = \frac{f}{2}\frac{dY_{in_p}(f)}{df} = \frac{N_{b_p}(f)}{D_{b_p}(f)} \tag{31}$$

where $N_{b_p}(f)$ and $Z_{p2}D(b_p f)$ are the numerator and denominator of the susceptance slope parameter $b_p(f)$, respectively,

$$
\begin{aligned}
N_{b_p}(f) = & \left(\theta_{p3}\frac{f}{f_{01}}\right)\left(\sec\left(\theta_{p3}\frac{f}{f_{01}}\right)\right)^2\left(Z_{p1}^2Z_{p2}^2\left(\tan\left(\theta_{p1}\frac{f}{f_{01}}\right)\right)^2\right. \\
& + 2Z_{p1}Z_{p2}(Z_{p2}^2 - Z_{p3}^2)\tan\left(\theta_{p1}\frac{f}{f_{01}}\right)\tan\left(\theta_{p2}\frac{f}{f_{01}}\right) + Z_{p2}^2Z_{p3}^2 \\
& + \left(Z_{p2}^4 + Z_{p1}^2Z_{p3}^2\left(\tan\left(\theta_{p1}\frac{f}{f_{01}}\right)\right)^2\right)\left(\tan\left(\theta_{p2}\frac{f}{f_{01}}\right)\right)^2\Big) \\
& + \left(\sec\left(\theta_{p2}\frac{f}{f_{01}}\right)\right)^2\left(\sec\left(\theta_{p3}\frac{f}{f_{01}}\right)\right)^2\left(Z_{p2}^3Z_{p3}\left(\theta_{p2}\frac{f}{f_{01}}\right)\right. \\
& + Z_{p1}^2Z_{p2}Z_{p3}\left(\theta_{p2}\frac{f}{f_{01}}\right)\left(\tan\left(\theta_{p1}\frac{f}{f_{01}}\right)\right)^2 \\
& \left. + Z_{p1}Z_{p2}^2Z_{p3}\left(\theta_{p1}\frac{f}{f_{01}}\right)\left(\sec\left(\theta_{p1}\frac{f}{f_{01}}\right)\right)^2\right), \\
D_{b_p}(f) = & 2Z_{p3}D_{Yin_p}(f)^2.
\end{aligned} \tag{32}
$$

In most previous works, only resonant conditions and slope parameters were considered, which means that only in-band responses were controlled. In our design, we wish to control the out-of-band performances simultaneously. Therefore, to suppress the undesired spurious (e.g., spikes) between two passbands and make the out-of-band cleaner, the transmission zeros $S_{21}(f_z)$ of the proposed TSSIR are also considered ($Z_0 = 50\,\Omega$),

$$|S_{21}(f_{z1})|^2 = \left|\frac{2}{2 + Y_{in_p}(f_{z1})Z_0}\right|^2 = 0, \tag{33}$$

$$|S_{21}(f_{z2})|^2 = \left|\frac{2}{2 + Y_{in_p}(f_{z2})Z_0}\right|^2 = 0. \tag{34}$$

Here, f_{z1} is the first transmission zero which should be set in between two passbands, and they are at or near certain same frequency. f_{z2} is the second transmission zero that is preferably set at or near certain same frequency beyond the second passband. Note that these considerations of transmission zeros are for each TSSIR, not for the whole filter yet.

There are 6 unknown variables of TSSIR, i.e., Z_{p1}, Z_{p2}, Z_{p3}, θ_{p1}, θ_{p2}, and θ_{p3} and 6 simultaneous Equations (4)–(11), (33)–(34). We can solve these 6 equations to obtain the 6 variables' values. In practice, if it is difficult to achieve exact zero in these equations, they can be approximated as 0 (or minimized) in order to find the unknowns.

2.4. Stepped-Impedance Inverter

The dual-band inverter we adopted is stepped-impedance inverter (SII) by using three section stepped-impedance transmission lines, as shown in Fig. 3. The $ABCD$ of the proposed structure can be calculated by

$$
\begin{aligned}
\begin{bmatrix} A_J(f) & B_J(f) \\ C_J(f) & D_J(f) \end{bmatrix} = & \begin{bmatrix} \cos(\theta_1^{J_{k,k+1}}\frac{f}{f_{01}}) & jZ_1^{J_{k,k+1}}\sin(\theta_1^{J_{k,k+1}}\frac{f}{f_{01}}) \\ jY_1^{J_{k,k+1}}\sin(\theta_1^{J_{k,k+1}}\frac{f}{f_{01}}) & \cos(\theta_1^{J_{k,k+1}}\frac{f}{f_{01}}) \end{bmatrix} \\
& \begin{bmatrix} \cos(\theta_2^{J_{k,k+1}}\frac{f}{f_{01}}) & jZ_2^{J_{k,k+1}}\sin(\theta_2^{J_{k,k+1}}\frac{f}{f_{01}}) \\ jY_2^{J_{k,k+1}}\sin(\theta_2^{J_{k,k+1}}\frac{f}{f_{01}}) & \cos(\theta_2^{J_{k,k+1}}\frac{f}{f_{01}}) \end{bmatrix} \\
& \begin{bmatrix} \cos(\theta_1^{J_{k,k+1}}\frac{f}{f_{01}}) & jZ_1^{J_{k,k+1}}\sin(\theta_1^{J_{k,k+1}}\frac{f}{f_{01}}) \\ jY_1^{J_{k,k+1}}\sin(\theta_1^{J_{k,k+1}}\frac{f}{f_{01}}) & \cos(\theta_1^{J_{k,k+1}}\frac{f}{f_{01}}) \end{bmatrix}
\end{aligned} \tag{35}
$$

$$
\begin{aligned}
A_J(f) &= \left(\cos\left(2\theta_1^{J_{k,k+1}}\frac{f}{f_{01}}\right)\cos\left(\theta_2^{J_{k,k+1}}\frac{f}{f_{01}}\right)\right. \\
&\quad \left.-\sin\left(2\theta_1^{J_{k,k+1}}\frac{f}{f_{01}}\right)\sin\left(\theta_2^{J_{k,k+1}}\frac{f}{f_{01}}\right)\left(R_{c_{J_{k,k+1}}}+1/R_c^{J_{k,k+1}}\right)\right)\Big/2 \\
&= D_J, \qquad (36)\\
B_J(f) &= jZ_2^{J_{k,k+1}}\left(R_c^{J_{k,k+1}}\sin\left(2\theta_1^{J_{k,k+1}}\frac{f}{f_{01}}\right)\cos\left(\theta_2^{J_{k,k+1}}\frac{f}{f_{01}}\right)\right. \\
&\quad -\left(R_c^{J_{k,k+1}}\right)^2\sin\left(\theta_2^{J_{k,k+1}}\frac{f}{f_{01}}\right) \\
&\quad \left.+\left(\left(R_c^{J_{k,k+1}}\right)^2+1\right)\cos(\theta_1^{J_{k,k+1}}\frac{f}{f_{01}})^2\sin\left(\theta_2^{J_{k,k+1}}\frac{f}{f_{01}}\right)\right), \qquad (37)\\
C_J(f) &= j\frac{1}{Z_2^{J_{k,k+1}}}\left(\sin\left(2\theta_1^{J_{k,k+1}}\frac{f}{f_{01}}\right)\cos\left(\theta_2^{J_{k,k+1}}\frac{f}{f_{01}}\right)/R_c^{J_{k,k+1}}\right. \\
&\quad -\sin\left(\theta_2^{J_{k,k+1}}\frac{f}{f_{01}}\right)/\left(R_c^{J_{k,k+1}}\right)^2 \\
&\quad \left.+\cos\left(\theta_1^{J_{k,k+1}}\frac{f}{f_{01}}\right)^2\sin\left(\theta_2^{J_{k,k+1}}\frac{f}{f_{01}}\right)/\left(1+1/\left(R_c^{J_{k,k+1}}\right)^2\right)\right). \qquad (38)
\end{aligned}
$$

where $f = f_{01}$ or f_{02}. With reference to Fig. 3, $\theta_1^{J_{k,k+1}}$ and $\theta_2^{J_{k,k+1}}$ are the electrical lengths of the inverter sections at f_{01}. $R_c^{J_{k,k+1}}$ is the characteristic impedance ratio of the inverter sections,

$$R_c^{J_{k,k+1}} = Z_1^{J_{k,k+1}}/Z_2^{J_{k,k+1}}. \qquad (39)$$

In the previous dual-band inverters, following the definition of ideal inverter, the considerations are usually

$$|B_J(f_{01})| = \frac{1}{J_{k_1,k_1+1}^{f_{01}}}, \qquad (40)$$

$$|B_J(f_{02})| = \frac{1}{J_{k_2,k_2+1}^{f_{02}}}, \qquad (41)$$

$$A_J(f_{01}) = 0, \qquad (42)$$

$$A_J(f_{02}) = 0. \qquad (43)$$

However, these considerations alone cannot provide symmetric passband responses. Therefore, we introduce new considerations of the inverter to make the passband performance symmetric. Referring to the traditional single-band quarter-wavelength inverters in Fig. 1 and Fig. 2, the B absolute values of their corresponding $ABCD$s are $1/J_{k_1,k_1+1}^{f_{01}}$ and $1/J_{k_2,k_2+1}^{f_{02}}$, and they are local maxima at f_{01} and f_{02} also, while the A values are 0. These can ensure their respective passband has symmetric response. Thus, for the proposed SII, which is a dual-band inverter, the $B_J(f)|_{f=f_{01},f_{02}}$ absolute values should also be the local maxima with $dB_J(f)/df = 0$, so Eqs. (40) and (41) can be modified as

$$\left(|B_J(f_{01}| - \frac{1}{J_{k_1,k_1+1}^{f_{01}}}\right)^2 + \gamma\left|\frac{dB_J(f)}{df}\right|^2\Bigg|_{f=f_{01}} = 0, \qquad (44)$$

$$\left(|B_J(f_{02})| - \frac{1}{J_{k_2,k_2+1}^{f_{02}}}\right)^2 + \gamma\left|\frac{dB_J(f)}{df}\right|^2\Bigg|_{f=f_{02}} = 0, \qquad (45)$$

where γ is certain scale factor. Note that $J_{k_1,k_1+1}^{f_{01}}$ and $J_{k_2,k_2+1}^{f_{02}}$ can be different in order to realize different prototypes or orders. Meanwhile, following the definition of ideal inverter, the values of $A_J(f)|_{f=f_{01},f_{02}}$ should satisfy Eqs. (42) and (43).

Based on these requirements in Eqs. (42)–(45), the 4 unknown variables of SII, i.e., $Z_1^{J_{k,k+1}}$, $Z_2^{J_{k,k+1}}$, $\theta_1^{J_{k,k+1}}$ and $\theta_2^{J_{k,k+1}}$ can be solved directly. Again in practice, it may be difficult to achieve 0 exactly. Thus, those equations can be approximated as 0 in order to find the solution within an acceptable tolerance.

3. DUAL-ORDER FILTER WITH DIFFERENT RESPONSES

In this section, two dual-order filters with different responses are introduced. These two filters are designed and fabricated on a 25 mil Taconic RF-60A substrate with dielectric constant $\varepsilon_r = 10.5$. The via diameter is set to be 0.6 mm.

3.1. Example I

Example I is a dual-order filter with $N_1 > N_2$. The detailed specifications of both passbands are:

- Lowpass prototype responses: Passband 1 — Chebyshev (0.1 dB passband ripple), Passband 2 — Chebyshev (0.05 dB passband ripple).
- Orders: $N_1 = 5$, $N_2 = 3$.
- Center frequencies: $f_{01} = 1.8$ GHz, $f_{02} = 5.8$ GHz.
- Fractional bandwidths: $\Delta_1 = 0.7$ (1.17 GHz–2.43 GHz), $\Delta_2 = 0.15$ (5.37 GHz–6.24 GHz).

For simplicity, the corresponding individual single-band filters are selected as Π-type structures. Because the 5th order passband needs two more resonators than the 3rd order one, we assume that the first (TSSIR_1) and last (TSSIR_5) resonators are only needed to realize the passband with higher (5th) order. Therefore, for the first (5th order) passband, $\text{TSSIR}_1 = \text{TSSIR}_5$ should have their first resonances at f_{01}, and satisfy the required susceptance slope parameters at f_{01} ($b_1(f_{01}) = b_1^{f_{01}}$). However, for the second (3rd order) passband, TSSIR_1 and TSSIR_5 should have their second resonances $f_{R2} = f_s$ being pushed away to avoid interference. In this example, the second resonances f_s of TSSIR_1 and TSSIR_5 are set at 6.6 GHz. As we know, a smaller slope parameter of the resonator would give a wider passband. Thus, to reduce the attenuation from TSSIR_1 and TSSIR_5 at f_{02}, the susceptance slope parameter at f_s ($b_1(f_s)$) should be as small as possible. Because the 3rd order passband needs two inverters fewer, $J_{01}^{f_{02}}$ and $J_{34}^{f_{02}}$ in Fig. 2 can be corresponding to extended feeding lines with electrical lengths $\lambda/4$ at f_{02} and characteristic impedances Z_0. Thus, referring to Eqs. (22) and (23), $J_{12} = J_{45}$ in Fig. 3 should be $J_{12}(f_{02}) = J_{45}(f_{02}) = J_{01}^{f_{02}} = J_{34}^{f_{02}} = 1/Z_0$ at f_{02}, while $J_{12}(f_{01}) = J_{45}(f_{01}) = J_{12}^{f_{01}} = J_{45}^{f_{01}}$ at f_{01}.

Table 1 lists the calculated parameters of the two single-band bandpass filters. From this table, we can also find that the characteristic impedances of $Z_{n_2}^{f_{02}}$ (where $n_2 = 1$ to 3) are too small to be realized, but TSSIRs in our case can be realized readily. For TSSIR_1 and TSSIR_5, considering the fabrication limitations, we set the susceptance slope parameter ratio to be $b_p(f_{01})/b_p(f_s) = 0.56$. To suppress the spikes between two passbands and improve the out-of-band performance, the first transmission zeros of TSSIRs are set at 3.6 GHz. The second transmission zeros of TSSIR_2, TSSIR_3 and TSSIR_4 are set at 7 GHz. Because the second resonances f_s of TSSIR_1 and TSSIR_5 have been set at 6.6 GHz, which are too close to 7 GHz, the second transmission zeros of TSSIR_1 and TSSIR_5 are set at 8.5 GHz. By solving Eqs. (4)–(11), (33)–(34), all parameters of TSSIRs can be found, which are listed in Table 2.

The calculated parameters of dual-band resonators TSSIRs and dual-band inverters SIIs of Example I are listed in Table 2. The final dimensions in Fig. A1 along with the initial dimensions in Table A1 can be found in Appendix A. The theoretical, simulated and measured results are shown in Fig. 4, and one can find that they are in good agreement. To show the effect of all transmission zeros, the frequency rang shown in Fig. 4(a) is from 0 to 9 GHz. From Fig. 4(a), the transmission zeros can be found around 7 GHz and 8.5 GHz. The photo is also shown in the inset of Fig. 4.

3.2. Example II

Example II is a dual-order filter with $N_1 < N_2$ and the absolute bandwidth of the second passband wider than that of the first passband. The detailed specifications of both passbands are:

Table 1. Calculated parameters of the two single-band BPFs of Example I.

Low Passband		High Passband			
$J_{12}^{f_{01}} = J_{45}^{f_{01}}$	1/38.66	$J_{01}^{f_{02}} = J_{34}^{f_{02}}$	1/50	$J_{12}^{f_{01}}/J_{01}^{f_{02}}$	1.29
$J_{23}^{f_{01}} = J_{34}^{f_{01}}$	1/35.87	$J_{12}^{f_{02}} = J_{23}^{f_{02}}$	1/56.25	$J_{23}^{f_{01}}/J_{12}^{f_{02}}$	1.57
$b_1^{f_{01}} = b_5^{f_{01}}$	0.0134				
$b_2^{f_{01}} = b_4^{f_{01}}$	0.0263	$b_1^{f_{02}} = b_3^{f_{02}}$	0.1044	$b_2^{f_{01}}/b_1^{f_{02}}$	0.2517
$b_3^{f_{01}}$	0.0257	$b_2^{f_{02}}$	0.0921	$b_3^{f_{01}}/b_2^{f_{02}}$	0.2788
$Z_1^{f_{01}} = Z_5^{f_{01}}$	58.43 Ω			Z_0	50 Ω
$Z_2^{f_{01}} = Z_4^{f_{01}}$	29.89 Ω	$Z_1^{f_{02}} = Z_3^{f_{02}}$	7.52 Ω		
$Z_3^{f_{01}}$	30.59 Ω	$Z_2^{f_{02}}$	8.53 Ω		

Table 2. Calculated TSSIRs and SIIs of Example I.

SII	$Z_1^{J_{12}} = Z_1^{J_{45}}$	40.25 Ω	$Z_2^{J_{12}} = Z_2^{J_{45}}$	15.51 Ω		
	$Z_1^{J_{23}} = Z_1^{J_{34}}$	39.20 Ω	$Z_2^{J_{23}} = Z_2^{J_{34}}$	13.23 Ω		
	$\theta_1^{J_{12}} = \theta_1^{J_{45}}$	40.24°	$\theta_2^{J_{12}} = \theta_2^{J_{45}}$	3.35°		
	$\theta_1^{J_{23}} = \theta_1^{J_{34}}$	38.58°	$\theta_2^{J_{23}} = \theta_2^{J_{34}}$	5.33°		
TSSIR	$Z_{11} = Z_{51}$	81.79 Ω	$Z_{12} = Z_{52}$	30.07 Ω	$Z_{13} = Z_{53}$	66.82 Ω
	$Z_{21} = Z_{41}$	32.70 Ω	$Z_{22} = Z_{42}$	23.08 Ω	$Z_{23} = Z_{43}$	44.98 Ω
	Z_{31}	33.34 Ω	Z_{32}	25.39 Ω	Z_{33}	40.98 Ω
	$\theta_{11} = \theta_{51}$	39.45°	$\theta_{12} = \theta_{52}$	11.33°	$\theta_{13} = \theta_{53}$	27.20°
	$\theta_{21} = \theta_{41}$	58.29°	$\theta_{22} = \theta_{42}$	17.88°	$\theta_{23} = \theta_{43}$	9.21°
	θ_{31}	56.23°	θ_{32}	20.56°	θ_{33}	10.31°

• Lowpass prototype responses: Passband 1 — Butterworth, Passband 2 — Chebyshev (0.2 dB passband ripple).

• Orders: $N_1 = 4$, $N_2 = 5$.

• Center frequencies: $f_{01} = 1.8$ GHz, $f_{02} = 5$ GHz.

• Fractional bandwidths: $\Delta_1 = 0.4$ (1.44 GHz–2.16 GHz), $\Delta_2 = 0.2$ (4.5 GHz–5.5 GHz).

According to the specifications, Table 3 lists the calculated parameters of the corresponding individual single-band bandpass filters. In this example, we use TSSIR_1 to TSSIR_4 to realize the lower passband. TSSIR_5 is only used to implement the higher passband. Therefore, to avoid the influence of the first resonance of TSSIR_5 on lower passband, its first resonance $f_{R1} = f_s$ is set as 1.44 GHz and the second resonance is set as f_{02}. Meanwhile, its corresponding susceptance slope parameter ratio is set as $b_p(f_s)/b_p(f_{02}) = 0.12$. The first transmission zeros of all these 5 TSSIRs are set at 3.7, 3.7, 3.7, 4.1 and 3.9 GHz. The second transmission zeros are set as 6.6, 6.6, 6.6, 6.5 and 6.5 GHz, respectively. Thus, we can find all the TSSIRs by solving Eqs. (12)–(19), (33)–(34). The calculated parameters are listed in Table 4. Because Z_{23} and Z_{33} are too small, the corresponding widths of microstrip transmission lines are wide. Therefore, we use a short taper line to connect TSSIR_2 and TSSIR_3 with SIIs. Because the 4th order passband needs one inverter less, referring to Fig. 2, $J_{01}^{f_{02}}$ can be omitted and $J_{45}^{f_{02}}$ can be corresponding to an extended feeding line with electrical length $\lambda/4$ at f_{01} and characteristic impedance

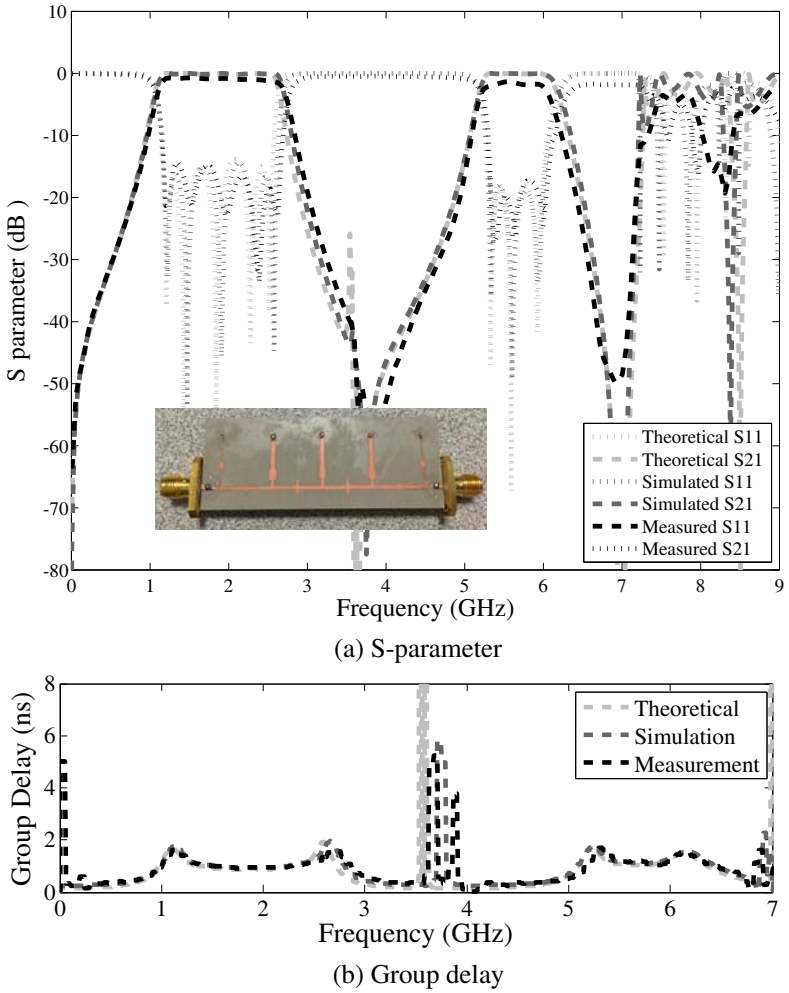

Figure 4. The theoretical, simulation and measurement results of Example I.

Z_0. Thus, referring to Eqs. (26) and (27), J_{45} in Fig. 3 should be equal to $J_{45}(f_{01}) = J_{45}^{f_{01}} = 1/Z_0$ at f_{01}, while $J_{45}(f_{02}) = J_{45}^{f_{02}}$ at f_{02}.

The initial dimensions can be found in Table A2 and the final dimensions of TSSIRs and SIIs after tuning can be found in Fig. A2 in Appendix A. The theoretical, simulation and measurement results of Example II are shown in Fig. 5. All the results can be found to be in a good agreement. The photo of Example II is also shown in the inset of Fig. 5. In theory, compared with Butterworth response, Chebyshev response has a worse group delay. From Fig. 5(b), we can see that the group delay of the first Butterworth passband is also better than that of the second Chebyshev passband.

Table 5 shows the comparison of simulation and measurement results of both examples including center frequencies, fractional bandwidths (Δ), Chebyshev passband ripples and Butterworth insertion loss (IL). From Table 5, we can observe that the simulation and measurement results are in good agreement.

Table 6 shows the comparison with other previous works. From this table, we can find that the separation between two passbands of this work is much farther than other works. For previous works, such as [10], [11] and [16], whose resonators were quarter-wavelength stub resonators, the separations between two passbands are very small. Even when the dual-band resonators were bisection SIRs in [9] and [19], the separations between two passbands are still smaller than 0.8. On the other hand, the separations of our examples can be larger than 1. Meanwhile, the prototype responses and orders of passbands in our examples can be different, unlike most other works with same or unspecified ones.

Table 3. Calculated parameters of the two single-band BPFs of Example II.

Low Passband		High Passband			
$J_{12}^{f_{01}}$	1/56.3613	$J_{12}^{f_{02}}$	1/36.2404	$J_{12}^{f_{01}}/J_{12}^{f_{02}}$	0.6430
$J_{23}^{f_{01}}$	1/63.5319	$J_{23}^{f_{02}}$	1/33.4338	$J_{23}^{f_{01}}/J_{23}^{f_{02}}$	0.5263
$J_{34}^{f_{01}}$	1/56.3613	$J_{34}^{f_{02}}$	1/33.4338	$J_{34}^{f_{01}}/J_{34}^{f_{02}}$	0.5932
$J_{45}^{f_{01}}$	1/50	$J_{45}^{f_{02}}$	1/36.2404	$J_{45}^{f_{01}}/J_{45}^{f_{02}}$	0.7248
$b_1^{f_{01}}$	0.0257	$b_1^{f_{02}}$	0.1130	$b_1^{f_{01}}/b_1^{f_{02}}$	0.2276
$b_2^{f_{01}}$	0.0488	$b_2^{f_{02}}$	0.2113	$b_2^{f_{01}}/b_2^{f_{02}}$	0.2325
$b_3^{f_{01}}$	0.0488	$b_3^{f_{02}}$	0.2098	$b_3^{f_{01}}/b_3^{f_{02}}$	0.2309
$b_4^{f_{01}}$	0.0257	$b_4^{f_{02}}$	0.2113	$b_4^{f_{01}}/b_4^{f_{02}}$	0.1218
		$b_5^{f_{02}}$	0.1130		
$Z_1^{f_{01}}$	30.2577 Ω	$Z_1^{f_{02}}$	6.9492 Ω	Z_0	50 Ω
$Z_2^{f_{01}}$	16.1020 Ω	$Z_2^{f_{02}}$	3.7178 Ω		
$Z_3^{f_{01}}$	16.1020 Ω	$Z_3^{f_{02}}$	3.7443 Ω		
$Z_4^{f_{01}}$	30.2577 Ω	$Z_4^{f_{02}}$	3.7178 Ω		
		$Z_5^{f_{02}}$	6.9492 Ω		

Table 4. Calculated TSSIRs and SIIs of Example II.

SII	$Z_1^{J_{12}}$	48.47 Ω	$Z_2^{J_{12}}$	66.73 Ω		
	$Z_1^{J_{23}}$	50.03 Ω	$Z_2^{J_{23}}$	75.88 Ω		
	$Z_1^{J_{34}}$	47.15 Ω	$Z_2^{J_{34}}$	67.87 Ω		
	$Z_1^{J_{45}}$	45.07 Ω	$Z_2^{J_{45}}$	58.32 Ω		
	$\theta_1^{J_{12}}$	32.43°	$\theta_2^{J_{12}}$	31.84°		
	$\theta_1^{J_{23}}$	31.94°	$\theta_2^{J_{23}}$	33.29°		
	$\theta_1^{J_{34}}$	32.40°	$\theta_2^{J_{34}}$	32.01°		
	$\theta_1^{J_{45}}$	32.73°	$\theta_2^{J_{45}}$	31.03°		
TSSIR	Z_{11}	21.89 Ω	Z_{12}	33.61 Ω	Z_{13}	27.20 Ω
	Z_{21}	10.95 Ω	Z_{22}	17.36 Ω	Z_{23}	14.11 Ω
	Z_{31}	10.67 Ω	Z_{32}	17.25 Ω	Z_{33}	14.00 Ω
	Z_{41}	15.24 Ω	Z_{42}	37.78 Ω	Z_{43}	22.22 Ω
	Z_{51}	10.00 Ω	Z_{52}	73.80 Ω	Z_{53}	35.94 Ω
	θ_{11}	32.85°	θ_{12}	39.44°	θ_{13}	23.07°
	θ_{21}	30.96°	θ_{22}	45.19°	θ_{23}	19.96°
	θ_{31}	30.29°	θ_{32}	47.48°	θ_{33}	18.70°
	θ_{41}	31.32°	θ_{42}	41.32°	θ_{43}	22.31°
	θ_{41}	17.93°	θ_{52}	50.63°	θ_{53}	20.07°

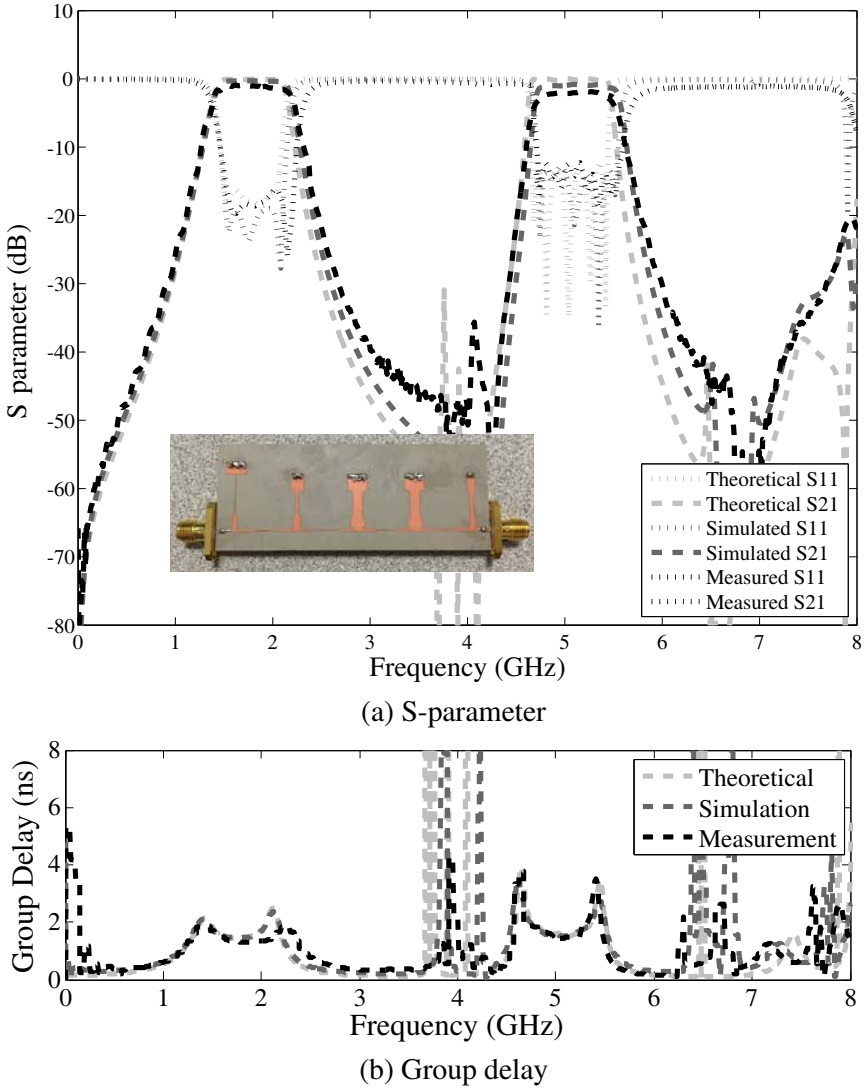

Figure 5. The theoretical, simulation and measurement results of Example II.

Table 5. Comparison of simulation and measurement results.

	f_{01}(GHz)		Δ_1(%)		Ripple (dB)/IL(dB)	
	Sim	Mea	Sim	Mea	Sim	Mea
Example I	1.76	1.77	72	70	0.18	0.21
Example II	1.75	1.75	38	39	0.4*	0.45*
	f_{02}(GHz)		Δ_2(%)		Ripple (dB)	
Example I	5.8	5.78	13	11	0.22	0.20
Example II	5.05	5.1	19	20	0.06	0.12

* For Butterworth passband, the values are the insertion losses.

Table 6. Comparison with other proposed dual-band filters.

	Specified Order/Prototype	Frequency (GHz)	Separation	Bandwidth (%)	Ripple (dB)/ IL (dB)	Upper-Stopband (GHz)
	1st & 2nd	f_{01} & f_{02}	$\frac{f_{02}-f_{01}}{\sqrt{f_{01}f_{02}}}$	Δ_1 & Δ_2	1st & 2nd	S_{21}@-10 dB
[7]	$-/-$&$-/-$	2.4 & 5.2	0.79	41 & 20	≈ 2 & ≈ 3	> 7
[8]	$-/-$ &$-/-$	0.9 & 1.93	0.78	22.22 & 3.1	1.1 & 1.8	> 2.5
[9]	$9/C_{0.1}$ & $9/C_{0.1}$	3.87 & 7.75	0.70	46.5 & 44.8	≈ 1 & ≈ 1	≈ 13
[10]	$2/-$ & $2/-$	1.5 & 2	0.29	5 & 4	1 & 4	≈ 3
[11]	$2/C_{0.01}$ & $2/C_{0.01}$	1.8 & 2.4	0.28	2.8 & 2.8	≈ 2 & ≈ 3	> 3
[13]	$2/-$ & $2/-$	2.3 & 4.8	0.79	10.3 & 6	2.77 & 2.88	> 10
[16]	$3/C_{0.1}$ & $3/C_{0.1}$	1.0 & 1.5	0.40	10 & 10	1.3 & 2.1	≈ 2.2
[19]	$2/B$ & $2/B$	2.4 & 5.2	0.79	54 & 20	0.4 & 0.8	≈ 8
[21]	$2/C$ & $2/C$	5 & 7.5	0.4	2 & 2	0.26 & 0.68	> 8
Example I	$5/C_{0.1}$ & $3/C_{0.05}$	1.8 & 5.8	1.20	72 & 13	0.2 & 0.2	> 7
Example II	$4/B$ & $5/C_{0.2}$	1.8 & 5	1.07	39 & 20	0.2 & 0.2	> 8

$-$:Not sepcified. B: Butterworth passband. $C_{0.1}$: Chebyshev passband with 0.1 dB passband ripple, etc.

4. CONCLUSION

This paper presents a novel design of dual-band filters with individually controllable passband responses and orders. Besides the center frequency and bandwidth, the response and order of each passband can be different and controlled individually. The dual-band filter has been formed by synthesizing each filter element (resonator, inverter) one by one, exploiting the corresponding individual single-band filters design tables/formulas for different prototype responses and orders. Trisection stepped-impedance resonators are adopted with novel considerations as dual-band resonators, whose additional design parameters could help to realize the required in-band responses (resonances, slope parameters) and improve simultaneously the out-of-band performances (transmission zeros of TSSIR). Furthermore, they can be used to design a dual-band filter with far separation between two passbands. Meanwhile, stepped-impedance inverters have been chosen as dual-band inverters with novel additional conditions to obtain symmetric passbands, which can also provide different inverter immittance parameters J/K at two center frequencies when the response or order of each passband is different. To illustrate the two passbands being controlled individually, two dual-band filters with different orders and responses have been demonstrated.

APPENDIX A.

The initial dimensions of both examples are given in Table A1 and Table A2. The final dimensions of both examples after tuning are shown in Fig. A1 and Fig. A2, units in mm. According to theoretical results of each TSSIR and SII, we can tune their initial widths and lengths in full-wave EM solver to obtain the similar results. After tuning TSSIRs and SIIs one by one, we can tune TSSIRs and SIIs together in full-wave EM solver to find the final dimensions according to the theoretical results of the whole structure.

Table A1. Initial dimensions of Example I (Units in mm).

SII	$W_1^{J12} = W_1^{J45}$	0.85	$L_1^{J12} = L_1^{J45}$	6.99		
	$W_2^{J12} = W_2^{J45}$	3.57	$L_2^{J12} = L_2^{J45}$	0.53		
	$W_1^{J23} = W_1^{J34}$	0.89	$L_1^{J23} = W_1^{J34}$	6.68		
	$W_2^{J23} = W_2^{J34}$	4.36	$L_2^{J23} = L_2^{J34}$	0.84		
TSSIR	$W_{11} = W_{51}$	0.13	$W_{12} = W_{52}$	1.33	$W_{13} = W_{53}$	0.26
	$W_{21} = W_{41}$	1.23	$W_{22} = W_{42}$	2.09	$W_{23} = W_{43}$	0.68
	W_{31}	1.19	W_{32}	1.82	W_{33}	0.82
	$L_{11} = L_{51}$	7.44	$L_{12} = L_{52}$	1.91	$L_{13} = L_{53}$	5.00
	$L_{21} = L_{41}$	9.91	$L_{22} = L_{42}$	2.94	$L_{23} = L_{43}$	1.62
	L_{31}	9.58	L_{32}	3.41	L_{33}	1.80

Table A2. Initial dimensions of Example II (Units in mm).

SII	W_1^{J12}	0.68	W_2^{J12}	0.38		
	W_1^{J23}	0.62	W_2^{J23}	0.25		
	W_1^{J34}	0.55	W_2^{J34}	0.17		
	W_1^{J45}	0.58	W_2^{J45}	0.26		
	L_1^{J12}	5.76	L_2^{J12}	5.62		
	L_1^{J23}	5.73	L_2^{J23}	5.90		
	L_1^{J34}	5.68	L_2^{J34}	6.22		
	L_1^{J45}	5.75	L_2^{J45}	5.85		
TSSIR	W_{11}	2.25	W_{12}	1.17	W_{13}	1.64
	W_{21}	5.48	W_{22}	3.09	W_{23}	4.02
	W_{31}	5.66	W_{32}	3.11	W_{33}	4.06
	W_{41}	3.65	W_{42}	0.95	W_{43}	2.21
	W_{51}	6.11	W_{52}	0.18	W_{53}	1.04
	L_{11}	5.37	L_{12}	6.72	L_{13}	3.85
	L_{21}	4.79	L_{22}	7.24	L_{23}	3.15
	L_{31}	4.68	L_{32}	7.60	L_{33}	2.95
	L_{41}	4.97	L_{42}	7.13	L_{43}	3.65
	L_{51}	3.46	L_{52}	11.78	L_{53}	4.31

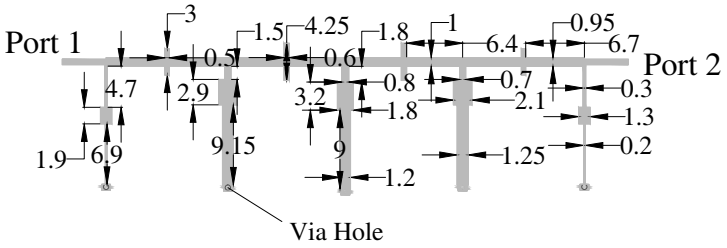

Figure A1. Final dimensions of Example I.

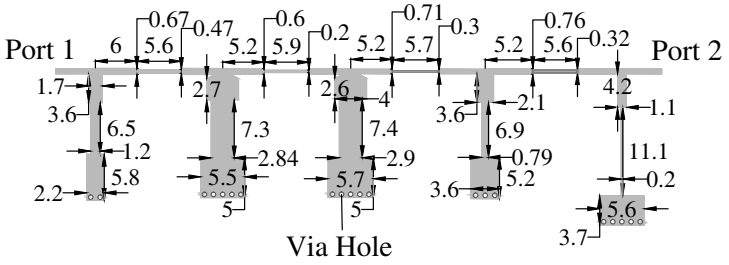

Figure A2. Final dimensions of Example II.

REFERENCES

1. Pozar, D. M., *Microwave Engineering*, 3rd edition, Wiley, New York, 2005.
2. Matthaei, G. L., L. Young, and E. M. T. Jones, *Microwave Filters, Impedance Matching Networks and Coupling Structures*, Ch. 8, Artech House, Norwood, MA, 1980.
3. Hong, J. S. and M. J. Lancaster, *Microstrip Filter for RF/Microwave Application.*, Wiley, New York, 2001.
4. Collin, R. E., *Foundations for Microwave Engineering*, 2nd edition, IEEE Press, 2001.
5. Lai, M.-I. and S.-K. Jeng, "Compact microstrip dual-band bandpass filters design using genetic-algorithm techniques," *IEEE Trans. Microwave Theory Tech.*, Vol. 54, 160–168, 2006.
6. Shang, X., Y. Wang, G. L. Nicholson, and M. J. Lancaster, "Design of multiple-passband filters using coupling matrix optimisation," *IET Microw. Antennas Propag.*, Vol. 6, 24–30, 2011.
7. Tsai, L.-C. and C.-W. Hsue, "Dual-band bandpass filters using equal-length coupled-serial-shunted lines and Z-transform technique," *IEEE Trans. Microwave Theory Tech.*, Vol. 53, 3265–3271, Apr. 2004.
8. Liu, Y. and W. Dou, "A dual-band filter realized by alternately connecting the main transmission-line with shunt stubs and shunt serial resonators," *IEEE Microw. Wireless Compon. Lett.*, Vol. 19, 296–298, 2009.
9. Liu, A.-S., T.-Y. Huang, and R.-B. Wu, "A dual wideband filter design using frequency mapping and stepped-impedance resonators", *IEEE Trans. Microwave Theory Tech.*, Vol. 56, 2921–2929, Dec. 2008.
10. Quendo, C., E. Ruis, and C. Person, "An original topology of dual-band filter with transmission zeros," *IEEE MTT-S Int. Microwave Symp. Dig.*, 1093–1096, Jun. 2003.
11. Guan, X., Z. Ma, P. Cai, Y. Kobayashi, T. Anada, and G. Hagiwara, "Synthesis of dual-band bandpass filters using successive frequency transformations and circuit conversions," *IEEE Microw. Wireless Compon. Lett.*, Vol. 16, 110–112, Mar. 2006.
12. Chaudhary, G., Y. Jeong, K. Kim, and D. Ahn, "Design of dual-band bandpass filters with controllable bandwidths using new mapping function," *Progress In Electromagnetics Research*, Vol. 124, 17–34, 2012.
13. Kim, C. H. and K. Chang, "Independently controllable dual-band bandpass filters using asymmetric stepped-impedance resonators", *IEEE Trans. Microwave Theory Tech.*, Vol. 59, 3037–3047, 2011.
14. Zhang, G.-Q., J.-X. Chen, J. Shi, H. Tang, H. Chu, and Z.-H. Bao, "Design of multilayer balun filter with independently controllable dual passbands," *IEEE Microw. Wirel. Compon. Lett.*, Vol. 25, 10–12, 2015.
15. Hu, C., X.-Z. Xiong, Y.-L. Wu, and C. Liao, "Design dual-mode bandpass filters based on symmetrical T-shaped stub-loaded stepped-impedance resonators with high frequencies selectivity", *Progress In Electromagnetics Research B*, Vol. 55, 325–345, 2013.
16. Tsai, C.-M., H.-M. Lee, and C.-C. Tsai, "Planar filter design with fully controllable second passband," *IEEE Trans. Microwave Theory Tech.*, Vol. 53, 3429–3439, Nov. 2005.

17. Lee, H.-M. and C.-M. Tsai,"Dual-band filter design with flexible passband frequency and bandwidth selections," *IEEE Trans. Microwave Theory Tech.*, Vol. 55, 1002–1009, May 2007.
18. Chin, K.-S., J.-H. Yeh, and S.-H. Chao, "Compact dual-band bandstop filters using stepped-impedance resonators," *IEEE Microw. Wireless Compon. Lett.*, Vol. 17, 849–851, Dec. 2007.
19. Chin, K. S. and J. H. Yeh, "Dual-wideband bandpass filter using short-circuited stepped-impedance resonators," *IEEE Microw. Wirel. Compon. Lett.*, Vol. 19, 155–157, 2009.
20. Makimoto, M. and S. Yamashita, *Microwave Resonators and Filters for Wireless Communication: Theory, Design and Application*, Springer-Verlag Berlin Heidelberg, 2001.
21. Naeem, U., S. Bila, M. Thevenot, T. Monediere, and S. Verdeyme, "A dual-band bandpass filter with widely separated passbands," *IEEE Trans. Microwave Theory Tech.*, Vol. 62, 450–456, 2014.
22. Sun, X. and E. L. Tan, "A novel dual-band bandpass filter using gerenalied trisection stepped impedance resonator with improved out-of-band performance," *Progress In Electromagnetics Research Letters*, Vol. 21, 31–40, 2011.
23. Sun, X. and E. L. Tan, "A dual-band bandpass filter using dual-band trisection stepped-impedance resonators and stepped-line inverters," *Asia-Pacific Microwave Conference Proceedings, APMC*, 908–911, 2011.
24. Sun, X. and E. L. Tan, "Novel dual-band dual-prototype bandpass filter," *Microwave and Optical Technology Letters*, Vol. 56, 1496–1498, 2014.